

Coherent Turning Behaviors Revealed Across Adherent Cells

Yiyu Zhang,^{1,2,*} Xiaoyu Yu,^{1,3,*} Boyuan Zheng,^{1,2} Ye Xu,³ Qihui Fan,^{1,†} Fangfu Ye,^{1,2,4,5,‡} and Da Wei^{1,§}

¹*Beijing National Laboratory for Condensed Matter Physics,*

Institute of Physics, Chinese Academy of Sciences, Beijing 100190, China

²*School of Physical Sciences, University of Chinese Academy of Sciences, Beijing 100049, China*

³*School of Mechanical Engineering & Automation, Beihang University, Beijing 100191, China*

⁴*Wenzhou Institute, University of Chinese Academy of Sciences, Wenzhou, Zhejiang 325000, China*

⁵*Oujiang Laboratory (Zhejiang Lab for Regenerative Medicine, Vision and Brain Health), Wenzhou, Zhejiang 325000, China*

Adherent cells have long been known to display two modes during migration: a faster mode that is persistent in direction and a slower one where they turn. Compared to the persistent mode, the turns are less studied. Here we develop a simple yet effective protocol to isolate the turns quantitatively. With the protocol, we study different adherent cells in different morphological states and find that, during turns, the cells behave as rotors with constant turning rates but random turning directions. To perform tactic motion, the cells bias the sign of turning towards the stimuli. Our results clarify the bimodal kinematics of adherent cell migration. Compared to the rotational-diffusion-based turning dynamics - which has been widely implemented, our data reveal a distinct picture, where turns are governed by a deterministic angular velocity.

Keywords: adherent cells, persistence, bimodal migration, mechanotaxis, persistent turning

INTRODUCTION

Cell migration is the basis of various physiological processes [1]. When migrating, cells have long been found to alternate between a persistent and a non-persistent mode [2, 3]. The persistent fractions are sometimes referred to as 'runs', which are driven by directional flow of actin filaments inside the cells [4]. The actin flow serves a pivotal role when a cell runs: it breaks the directional symmetry as the cell tends to migrate along the flow's direction; meanwhile, the flow's speed governs how fast the cell can move [5]. Moreover, the directional flow of actin and cell polarization enhance one another. Altogether, these interactions between cell speed, polarity, and actin flow result in a universal coupling between the cells' speed and persistence (UCSP) [5]. This model has been a powerful tool, as it offers a comprehensive framework that encompasses both sub-cellular and single-cellular dynamics.

Compared to the runs, the less persistent periods of cell migration, which are primarily responsible for the turning, are less studied [6–8]. However, they are no less important for cell migration. A primary reason for the scarcity of studies is that kinematics of turns are more complex than that of runs. While runs appear unambiguously as straight motions and this applies universally for different microorganisms (not limited to adherent tissue cells), turning behaviors manifest in a wide variety of forms. This is best exemplified by the colorful terms coined to describe microbial locomotion, such as 'run-and-tumble' [7, 9], 'run-and-circle' [6, 10], and 'run-

reverse-flick' [11]. Even within eukaryotic cells, turning may mean either a period of stronger rotational diffusion [7, 12] or a gradual but steady change in the cell's direction [6, 8]. Consequently, in experiments using different cells, turning behaviors are characterized in different ways, such as fitting to diffusive models [12, 13] or frame-to-frame comparison of directions [14, 15]. All the aforementioned varieties add up and make cross-comparison of results over cell types challenging, hindering us from obtaining a holistic view of how cell turns.

In this study, we focus on adherent eukaryotic cells and we aim to resolve their common turning kinematics. A unified framework is developed to assess turning behaviors across these cells. We find that, despite variability in cell type, size, and morphology, they all turn analogously to rotors with randomized direction (chirality) but constant turning rates. Experimentally, the following picture of cell migration is revealed. First of all, the cells switch between runs and turns at constant probability rates (i.e., 2-state Markovian process featured by exponential state interval distributions). While running, the angular diffusion is strongly suppressed so that the cell can move persistently along a specific direction. Upon the finish of a run, the sign of the following turn is randomly determined and does not change thereafter. Then, during the entire turn, the cell's direction of motion changes at a constant rate. Finally, when the turn ends, the ending direction will be taken by the run that follows. In this picture of migration, we further resolved that the cells achieves targeted motion (mechanotaxis in this case) by biasing the probability of turning signs. These observed kinematics offers a renewed and generalized perspective to model cell migration, with which we examine the UCSP model with an unequivocal definition of persistence. Moreover, a positive dependence between the turning rate and duration is also found over different cells, supporting the existence of actin-involved positive

* These authors contributed equally to this work.

† fanqh@iphy.ac.cn

‡ fye@iphy.ac.cn

§ weida@iphy.ac.cn

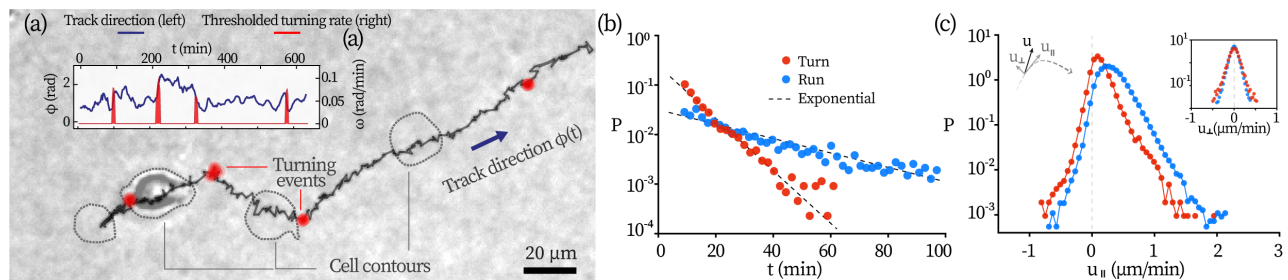


FIG. 1. Kinematics of MCF-10A migration on collagen substrates. (a) A typical track is displayed with the 'turns' marked red. The track's direction of motion and its thresholded turning rates are displayed in the inset. (b) The distribution of the state intervals. (c) The distributions of the cells' instantaneous velocities. The schematic drawing to the left displays how the velocity components are defined.

feedback loops hypothesized previously [6]. Our findings highlights the general applicability of constant-rate turns in adherent cell migration and contribute to a refined description of adherent cell kinematics.

RESULTS

Distinguishing the two states by turning rates

We begin with examining epithelial cells (MCF-10A) on collagen (2 mg/ml) substrates. After the cells have adhered to the substrate, image sequences are taken every 2 min for 6 h. From the video recording, we track the cell contours for each frame and report the geometric center as the cell's location. In total, $N=396$ motile tracks of single cells are collected, for details see Materials and methods.

A typical track together with detected cell contours are displayed in Fig. 1(a) and Supplementary Video (SV). (see more tracks in Fig. ??). Similar to previous reports [16], cells migrate in a pattern where persistent motions are interrupted by brief turning events. At first sight, this pattern resembles the 'run-and-tumble' motion displayed by bacteria [9] and immune cells [7]. We have therefore attempted to discern turns from runs by speed-based criteria, which are previously applied to determine tumble events [7, 9, 17]. The attempt was not successful because: (1) the cells' moving speed while turning is only slightly lower than the speed of their runs. (2) The cells' varying shapes (e.g. extension and retraction of protrusions) give rise to a transient high-speed component during both turning and running, which misleads the speed-based state marking algorithms.

However, we find that turning-rate-based algorithms effectively separate the two states. We compute the track direction $\phi(t)$ and its rate of change $\omega = d\phi/dt$ from the smoothed tracks, see the inset of Fig. 1(a). Turning events are marked by thresholding the absolute turning rate $|\omega| > \Omega_c$. This simple algorithm, requiring minimal tuning of Ω_c , works successfully across various cell types, ranging from tissue cells (e.g., MCF-10A and NIH-3T3) to cancer cells (e.g., MDA-MB-231). A generalized pro-

ocol for determining Ω_c and more information about the algorithm is detailed in Appendix A.

We find that the duration of runs and turns both follow exponential distributions, Fig. 1(b). The characteristic times for runs and turns are $\tau_{\text{turn}} = 8.2$ min and $\tau_{\text{run}} = 29.9$ min [18]. In other words, cells spend approximately 80% [$\tau_{\text{run}}/(\tau_{\text{turn}} + \tau_{\text{run}})$] of the time in persistent motion. This is starkly different from the motion of non-adherent cells on the same substrate, which appear to spend 80% of the time in a stationary tumbling state [7].

Figure 1(c) presents the speed distributions of the MCF-10A cells. To better resolve the kinematics, we further decompose the cells' instantaneous velocity \mathbf{u} along its direction of motion (u_{\parallel}) and perpendicular to the direction (u_{\perp}). While the instantaneous velocities are computed from frame-to-frame displacement, the direction of motion is computed from the cell's net migration over $N = 7$ frames, which corresponds to a sampling window of $t_{\text{win}} = 12$ min. This helps isolate the cell's net migration from the displacement resulting from its fast deformations. Details about the use of t_{win} can be found in Appendix A. Directions are illustrated by the schematic drawing to the left of Fig. 1(c). The parallel component, u_{\parallel} , generates effective forward migration. While u_{\parallel} is indeed larger for runs, its distributions for runs and turns largely overlap. We also see that there is a finite probability for u_{\parallel} to be negative and this marks the transient components due to the contraction of the cells' contours. The probability of having negative u_{\parallel} is higher when a cell turns, suggesting that more significant morphological changes are taking place during then. This is further supported by a stronger fluctuation (standard deviation) in contour perimeter during turns. For both runs and turns, the perpendicular component u_{\perp} distributes symmetrically with respect to 0, see the inset of Fig. 1(c). u_{\perp} is larger during turns (broader distribution) because it contributes to changes in the direction of migration.

Cells turn with random signs but at a constant rate

How do cells turn? From a kinematic perspective, the answer appears to be surprisingly simple: they turn at a

constant rate. Figure 2(a) presents how the direction of migration ϕ changes over time during some typical turns. For each turn, ϕ appears to vary linearly with time, thus featuring a near-constant rate of turning. Distributions of the turning rates are identical for turns of both signs, see Fig. 2(b) and inset.

The relationship between the total duration of a turn t_{turn} and the total angular change during it $\Psi = \phi(t_{\text{end}}) - \phi(0)$ are displayed in Fig. 2(c). The ensemble of dots represents $N=2458$ turning events collected from the tracks, and the squares represent the mean of binned data, $\langle \Psi \rangle$. A clear linear dependence of $\langle \Psi \rangle$ on t_{turn} is found: $\langle \Psi \rangle = \Omega_{\text{turn}} t_{\text{turn}}$. Least-square linear fitting gives $\Omega_{\text{turn}} = 0.160 \pm 0.003$ rad/min, where the uncertainty represents the standard error. Meanwhile, we observe that the distribution of Ψ becomes more dispersed for longer turns (larger t_{turn}). This can be seen from the widths of the probability distributions of Ψ in Fig. 2(c) inset: short ($t_{\text{turn}} \leq 8$ min, blue), intermediate ($t_{\text{turn}} \in (8, 16]$ min, purple), and long turning events ($t_{\text{turn}} \in (16, 32]$ min, red) have increasingly broadened distributions. In other words, longer turns have more variability around the expected angular change. Angular changes for runs are displayed in Fig. 2(d). Here $\Psi = \phi(t_{\text{run}}) - \phi(0)$ with t_{run} the duration of a single run. $\langle \Psi \rangle$ increases with t_{run} orders of magnitude more slowly than it does during turns. Quantitatively, the rate reads 0.006 rad/min and is ~ 30 times smaller than Ω_{turn} , and can originate from diffusion (Appendix B). Similarly, the inset of Fig. 2(d) displays the probability distributions of Ψ for short ($t_{\text{turn}} \leq 30$ min, blue), intermediate [$t_{\text{turn}} \in (30, 60]$ min, purple], and long runs [$t_{\text{turn}} \in (60, 120]$ min, red]. The dispersity also increases over time but it increases only slightly, much slower than its counterparts during turns.

It is intriguing to see that the cells, on an ensemble level, behave as noisy constant-rate rotors. We further resolve the noise level by computing the cells' angular auto-correlation functions (ACFs). Figure 2(e) displays the ensemble average ($\langle \cdot \rangle$) of single-cell ACF $\equiv \mathbf{n}(t') \cdot \mathbf{n}(0)$, with $\mathbf{n}(t')$ the unit vector of the cell's moving direction at time t' . The term $\mathbf{n}(t') \cdot \mathbf{n}(0)$ readily reduces to $\cos(\Delta\phi(t'))$ with $\Delta\phi(t') \equiv \phi(t') - \phi(0)$. We further assume that the noise is Gaussian and corresponds to a rotational diffusion coefficient of D_r . The Langevin equation for a noisy rotor with a persistent turning rate Ω reads $\dot{\phi} = \Omega + \zeta(t)$, with $\zeta(t)$ the noise that satisfies $\langle \zeta(0)\zeta(\tau) \rangle = 2D_r\delta(\tau)$ and δ the Dirac delta function. For such rotors, their average ACF evolves as:

$$\langle \text{ACF} \rangle = \langle \cos(\Delta\phi(t')) \rangle = e^{-D_r t'} \cos \Omega t' \quad (1)$$

For small Ω , that is, during runs, the ACF further reduces to $\langle \text{ACF} \rangle \approx e^{-D_r t'}$. The experimentally obtained ACFs for turns and runs follow these descriptions precisely, see Fig. 2(e). Fitting the ACFs of turns with Eq. (1) gives $\Omega_{\text{turn}} = 0.159$ rad/min, agreeing with the value obtained by linearly fitting of $\langle \Psi \rangle$ as a function of t_{turn} [0.160 rad/min, Fig. 2(c)]. The rotational coefficients for turns

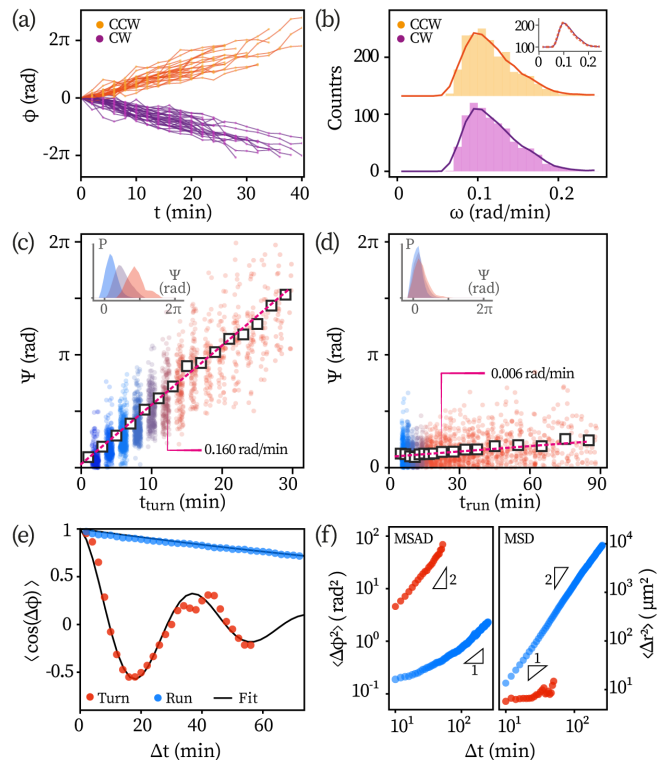


FIG. 2. Kinematics of turning. (a) How the migration direction ϕ vary with time during turns. CCW: counter-clockwise, CW: clockwise. (b) Probability distribution of turning rates. Inset: the histograms' contour overlaid. The total angular change during an event Ψ as a function of the event's duration ($t_{\text{turn,run}}$) with (c) for turns and (d) for runs, respectively. $N \sim 2000$ runs and turns are shown. Inset: probability distribution of Ψ for short, intermediate, and long events. (e) The angular correlation functions evolving over time. (f) Mean squared angular displacement (MSAD, left) and mean squared displacement (MSD, right) during the two states.

and runs read respectively $D_{r,\text{turn}} = 0.031$ rad²/min and $D_{r,\text{run}} = 0.004$ rad²/min. Notably, the angular noise is an order of magnitude lower for runs and shows why the distribution of Ψ maintains nearly the same dispersity over time, as displayed in Fig. 2(d) inset.

The message that the cells are alternating between being persistent runners and constant-rate rotors is echoed by other statistics, i.e., the mean square angular displacement ($\langle \Delta\phi^2 \rangle$, MSAD) and mean square displacement ($\langle \Delta r^2 \rangle$, MSD), Fig. 2(f). Angular changes (MSAD) accumulate near-ballistically over time for turns. For runs, notably, on time scales shorter than the events' characteristic duration τ_{run} (~ 30 min), MSAD only increases sub-diffusively, indicating a strong suppression of angular noise during runs. Only on time scales longer than τ_{run} , the angular changes start to build up diffusively. For spatial displacement, the trend is the opposite. MSD is ballistic for runs whereas (sub-)diffusive for turns.

We also examine whether single cells have their own characteristic turning rate or a preference for turning sign (Appendix C). We observe that the turning rates

of a single cell during its consecutive turns are highly randomized, and these rates are as scattered as those observed across an ensemble of cells [Fig. ??(a)]. The data does not support that single cells have characteristic turning rates. Also, they neither display a preferred sign of turning [Fig. ??(b)].

Mechanotaxis achieved by biasing the sign of turns

If a cell migrates only with two modes, namely, runs along an unchanged direction and turns at a constant rate, how does it perform targeted motion? An intuitive answer is that the cell can bias its direction of turning towards the stimuli to approach them. We now test this hypothesis.

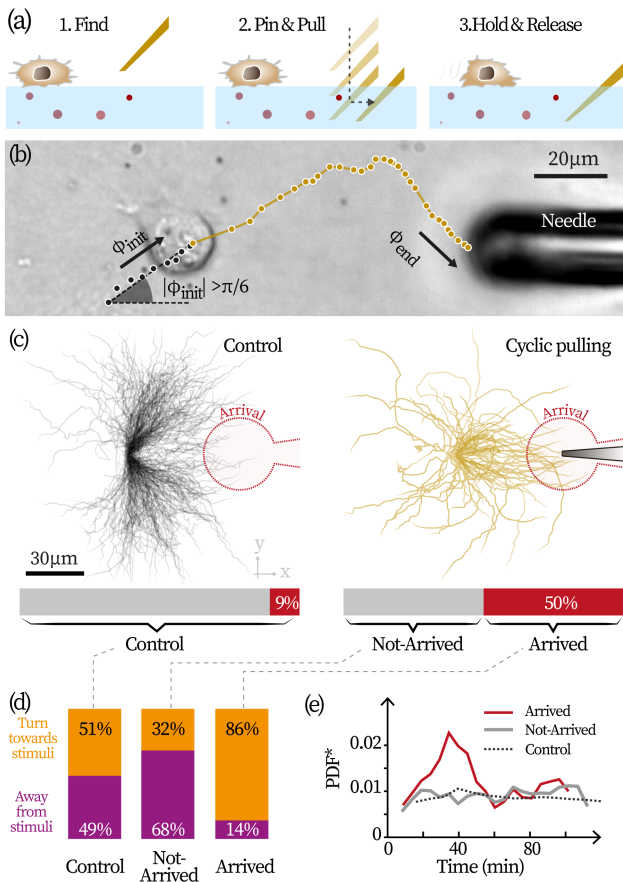


FIG. 3. Mechanotaxis of cells. (a) Experimental scheme for exerting cyclic pulling. (b) A typical eligible track of an attracted cell. The black segment represents pre-stimuli observation. (c) Visualization of eligible tracks in the control group (black, $N=293$) and tracks in mechanotaxis assays (yellow, $N=93$). The fraction of Cells arrived at the red-shaded areas are reported by bottom bars. (d) Directional distributions and (e) temporal distributions of turns in different cell groups. The distribution of arrived cells in (e) is adjusted to account for the tracks' varying duration, see Methods for detail.

Following a similar protocol as Ref. [7], cyclic pulling is applied to the substrate on which the cells are deposited,

serving as mechanical cues. In short, micropipettes were inserted into the collagen substrate 60 μ m to the right of the cell. They are then used to pull the substrates further rightwards, sustaining the stretch for some time. Lastly, the substrate is released and the pipette goes back to the initial location to start another cycle, see Fig. 3(a) for an illustration and see Methods for details.

We examine single-cell trajectories in response to the mechanical stimuli. Before insertion of the micropipette, we ensure that the candidate cell is motile and its moving direction does not point directly to the stimuli [$\phi(0) \notin [-\frac{\pi}{6}, \frac{\pi}{6}]$]. Moreover, because we observe that cells originally moving leftwards [$\phi(0) \in [\pm\frac{\pi}{2}, \pm\pi]$] do not get attracted to move to the pipette, thus we also exclude this angular range. A typical eligible track is displayed in Fig. 3(b), with the black fraction representing the cell's pre-stimuli migration and the yellow segment its motion after the stimuli is applied. Note that $\phi(0)$ is computed based on the cell's pre-stimuli trajectory. See also SV. 2 for an attracted cell. In total, $N = 93$ motile cells whose initial angles are in the desired range are gathered for this study. To comprise a control group, $N=293$ eligible tracks are collected. These cells are motile, have proper initial directions, and migrate with no pipette inserted into the substrate. The two groups of tracks are displayed in Fig. 3(c).

A cell is considered to be attracted if it has arrived at the pipette within 120 min, or its distance to the needle at the end of 120 min is smaller than 20 μ m. The region of arrival is visualized by the red-shaded area in Fig. 3(c). Compared to the control group where only 9% of cells ($N=26$ out of 293) arrived at the stimuli, $\sim 50\%$ cells ($N=47$ out of 93) under cyclic pulling of the substrate are attracted [the bars at the bottom of Fig. 3(c)]. Since this region has no actual difference from elsewhere for the control group, the arrival fraction should be interpreted as the baseline probability for an eligible cell to end up in such an area of complex geometry.

To resolve the direction of turning of cells under stimuli, we pool all detected turning events and divide them into three groups: the turns taken by the arrived cells, by the non-arrived cells, and additionally, those by the cells in control group (as a whole). A turn is considered helping the cell get closer to the stimuli if it decreases $\theta \equiv \arccos(\mathbf{n} \cdot \mathbf{n}_{c \rightarrow p})$, which denotes the included angle between the unit vector along a cell's moving direction, \mathbf{n} , and the unit vector pointing from the cell's location at the moment of turning, to the pipette tip, $\mathbf{n}_{c \rightarrow p}$.

Figure 3(d) displays the fractions of the turns that help cells move towards the stimuli (orange) or away from the stimuli (purple). While turns in the control group does not favor either sign, among the arrived cells, the turning sign is predominantly biased to help the cell migrate towards the stimuli (86%). To confirm whether the turning sign is biased due to mechanotactic responses, we benchmark the temporal distribution of the turns in the arrived group against the control group, see Fig. 3(e). In the control group, turns take place at a constant rate,

featuring a flat line in the turns' probability distribution over time. In sharp contrast, among the arrived cells, the probability peaks during the first ~ 50 min after the onset of stimuli (at $t=0$ min), meaning that the cells have become more likely to turn. Such responsiveness indicates that the majority of the arrived cells are actively engaged in mechanotaxis. In other words, the probability rates of turning show that the temporal symmetry is maintained in the control group, whereas it is broken in the arrived group by the introduction of external stimuli.

It is noteworthy that the cells under stimuli do not always respond to stimuli. The temporal distribution of turn of not-arrived cells shows no response to stimuli, remaining essentially the same as the control group, see Figs. 3(d) and 3(e). Meanwhile, their signs of turns are slightly biased away from the stimuli, possibly because some non-responsive cells that happen to arrived at the stimuli have been excluded.

To summarize, our data show that, upon exposure to mechanical stimuli, a considerable fraction of MCF-10A cells are attracted, although not all are responsive. For those responsive cells, their mechanotaxis is underpinned by biasing the overall direction of turning towards the stimuli.

Migration of mesenchymal MCF-10A and NIH-3T3 cells

Results shown so far indicate MCF-10A cells on collagen (~ 10 Pa), which are predominantly in the amoeboid morphology, switch between being persistent runners and constant-rate rotors. Cells in such morphology tend to migrate without mature focal adhesions and stress fibers [19]. On different substrates, the cells' motility and morphology can be different [20]. We therefore examine MCF-10A on stiffer substrates (PDMS, 750 kPa). In this case, the cells migrate in a mesenchymal fashion: they adopt an elongated, spindle-like shape and exert traction on their substrates via focal adhesions associated with actin-rich protrusions, such as lamellipodia or filopodia [21]. We find that the runner-rotor model still precisely captures the cells' migration kinematics.

In total, $N=318$ motile MCF-10A cells are examined on PDMS. The fluorescent image of a typical MCF-10A in mesenchymal mode is displayed in Fig. 4(a). The cells' different morphological can be seen straightforwardly from the significant difference in the cells' aspect ratio (AR) [inset of Fig. 4(a), $p < 0.001$ by Kruskal-Wallis test, one-way ANOVA]. We define AR as the ratio of the longest side to the shortest side of the smallest bounding box of the cell's outline. Cells examined on collagen have concentrated around $AR = 1$, while on PDMS, they have AR distributed between 1 and 2 in a nearly uniform fashion.

The mesenchymal cells also have exponentially distributed state intervals for runs and turns, Fig. 4(b). In these cells, a run persists approximately twice as long

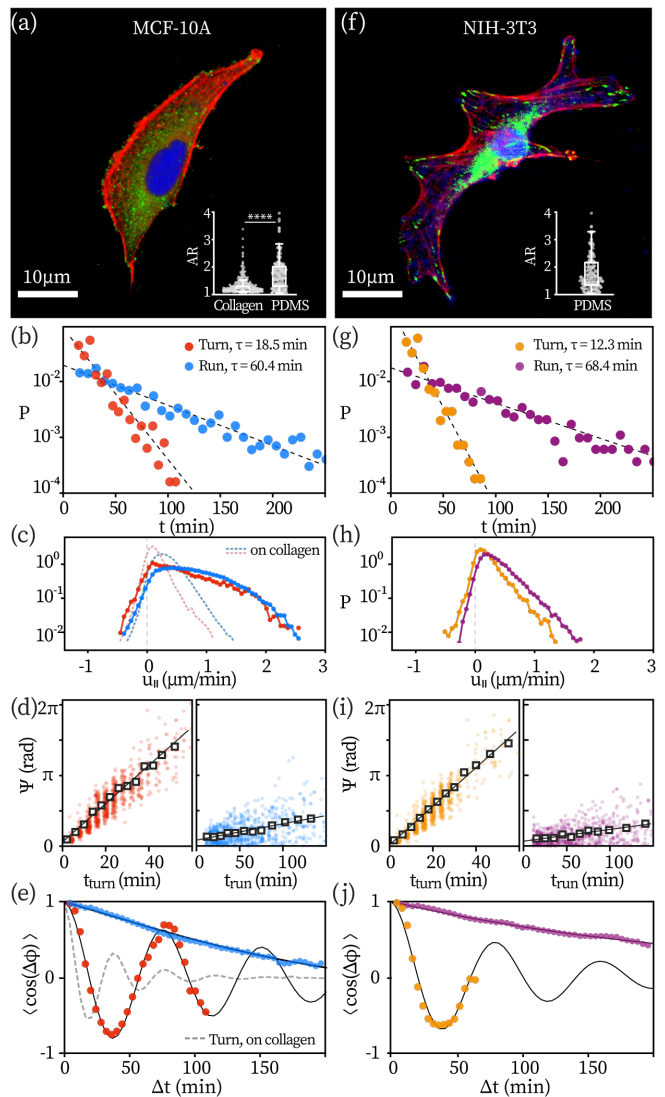


FIG. 4. Runner-rotor motility in other cells. (a) Fluorescent microscopy of MCF-10A cell examined on PDMS substrates. Inset: comparison of aspect ratio (AR) between cells examined on different substrates. ****: $p < 0.001$, Kruskal-Wallis test, one-way ANOVA. Distributions of duration (b) and velocity along the track direction (c) for turns and runs. (d) Total change in direction, Ψ , as a function of a state's duration. (e) Angular auto-correlation function for both states. Data are fitted exponentially in b (dashed line), linearly in f (solid line), and by Eq. (1) in e (solid line). Panel (f)-(j) respectively show information of NIH-3T3 cells in the same form as (a)-(e).

as in their amoeboid counterparts. Mesenchymal MCF-10A cells also run faster: $\bar{V}_{\text{run}} = 0.76 \pm 0.32 \mu\text{m}/\text{min}$ (mean \pm std.) versus $0.39 \pm 0.16 \mu\text{m}/\text{min}$ for cells on collagen. Figure 4(c) further resolves the distribution of the velocity component parallel to the cell's moving direction, during both turns (red solid line) and runs (blue solid line). Both traces reach further to the positive values compared to the amoeboid data (dashed lines), indicating much enhanced motility.

Nevertheless, on the ensemble level, cells still turn at a
 near-constant rate ($\Omega_{\text{turn}} = 0.090 \pm 0.003$ rad/min) and is
 an order of magnitude faster than they do in runs (0.007
 rad/min), see the left and right panels in Fig. 4(d) respec-
 tively. Fitting the cells' ACF with Eq. (1) [solid lines in
 Fig. 4(e)] gives essentially the same turning rate. For the
 sake of space and clarity, comprehensive fitting results
 are summarized in Table I. Notably, the mesenchymal
 cells turn with much stronger coherence than the amoeboid
 cells, which can be directly seen from Fig. 4(e),
 that the oscillatory pattern of ACF lasts much longer
 than for the cells examined on collagen (dashed line).
 Quantitatively, the turning noise in mesenchymal cells
 ($D_{r,\text{turn}} = 0.005$ s $^{-1}$) amounts to less than 20% of the
 noise in amoeboid cells (0.031 s $^{-1}$).

Clearly, the runner-rotor model applies precisely for
 MCF-10A cells in mesenchymal state. These cells with
 stronger morphological polarity [Fig. 4(a) inset] are found
 to run more persistently and faster [Figs. 4(b) and 4(c)].
 Meanwhile, they are subjected to much less rotational
 noise during turns [Fig. 4(e)]. This is in line with the
 UCSP model [5], that cell polarity, speed, and persistence
 are positively correlated.

Does the runner-rotor kinematics observed in epithelial
 cells (MCF-10A) applies for other cells? We examined
 the well-characterized fibroblast cell (NIH-3T3, $N=280$)
 cells on the same PDMS substrate. The cells display a
 morphology similar to the MCF-10A cells, Fig. 4(f) and
 inset. The state intervals of NIH-3T3 again follow two ex-
 ponential distributions, in line with previous study [15],
 Fig. 4(g). Results on the cells' motility, turning rates,
 and the coherence of turning are presented in Figs. 4(h),
 4(i), and 4(j) respectively. These results are analogous to
 those obtained from MCF-10A cells, see Table I for the
 parameters of fitting. The precision of applying the cur-
 rent framework to another type of cell evidences the gen-
 eral applicability of the runner-rotor kinematics. Typical
 migration of MCF-10A and NIH-3T3 cells can be found
 in SV. 3 and 4 respectively.

UCSP revisited and the coupling between turning rate and duration

Conventionally, a cell's persistence is measured often
 in an *ad hoc* fashion. In some cases, persistence is ex-
 perimentally measured as the time needed for a cell to
 turn 90° [5, 22]; or the total time span where frame-to-
 frame turning angle is less than 30° [14, 15]; or obtained
 by fitting tracks [12, 13] or MSDs to models [23]. While
 these practices have generated valuable insights in their
 respective systems, the variability makes cross-cell com-
 parison difficult. In this section, we show the insights
 brought about by the runner-rotor kinematics and its
 implications for the UCSP model.

Given a cell is constantly switching between running
 and turning, the practice of reporting persistence as the
 time corresponds to 90°-change in migration direction

would result in large uncertainty, because the reported
 value strongly depends on where the measurement starts.
 Moreover, by modeling runner-rotor kinematics, we find
 that, when persistence is reported as such, the typical
 exponential dependence of persistence on the speed [5],
 which are used to justify UCSP, does not suffice this pur-
 pose. In fact, the exponential dependence may mani-
 fest even without any coupling between persistence and
 speed, Fig. ???. Detailed information can be found in
 Appendix D.

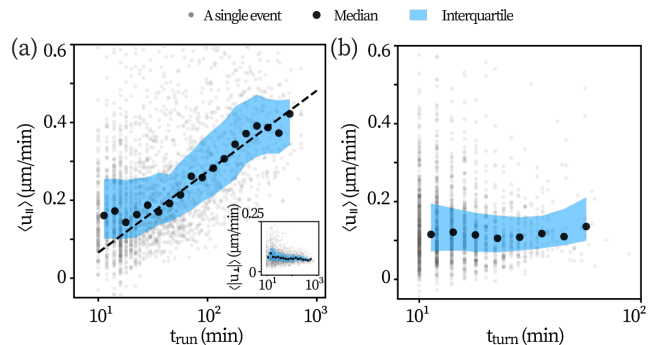


FIG. 5. UCSP examined with cell migration dichotomized as runs and turns. (a) Correlation between cell speed and the duration of runs ($N=2413$) and (b) turns ($N=1657$) that are longer than 10 min.

On the other hand, the runner-rotor model gives an unambiguous definition of persistence time: the duration of a run t_{run} . With this refined definition, we re-examine if the cells' speed and persistence are coupled. We again decompose the cells' instantaneous velocity as u_{\perp} and u_{\parallel} . Figure 5(a) displays the results of runs collected from MCF-10A cells on collagen. Each dot in the background represents a run event, while the black circles and the shading represent respectively the median and interquartile of the data binned by t_{run} . The mean effective component for forward-motion, $\langle u_{\parallel} \rangle$, is found to be strongly coupled with the total duration of run t_{run} , see Fig. 5(a); whereas the perpendicular component, $\langle u_{\perp} \rangle$ is not coupled with t_{run} , see Fig. 5(a) inset. Data for MCF-10A and NIH-3T3 cells tested on PDMS substrates show qualitatively the same results. Altogether, these results provide a solid and nuanced support to the UCSP model.

Naturally, it is also of interest to see if migration speed is also correlated with the duration of turns. Figure 5(b) shows the relationship between $\langle u_{\parallel} \rangle$ and the total duration of turn (t_{turn}) from MCF-10A cells on collagen. How fast a cell moves during turns appears to have no correlation with how long this turn would last. Next, instead of analyzing how t_{turn} is correlated to the perpendicular speed component u_{\perp} , which fluctuates strongly over time due to the cells' morphological changes, it is more instructive to directly analyze the correlation between the angular velocity (ω) and the duration t_{turn} of a turn.

In a previous study using fish keratocyte [6], it is suggested that the turning rate and its duration are mutually

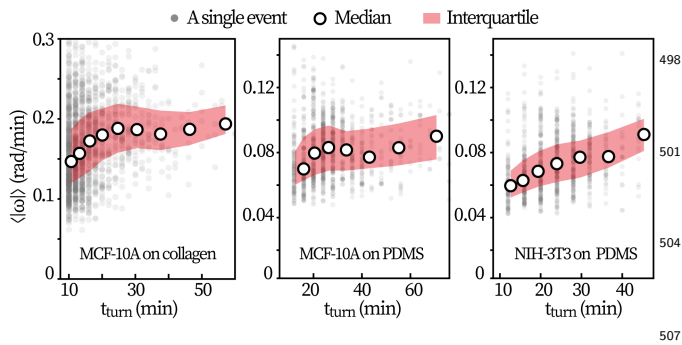


FIG. 6. Positive correlation between the rate and duration of turns. Panels correspond respectively to different dataset as annotated. Note that the x -axes are linear.

enhancing factors. Indeed, although turning rates within a dataset only vary within a small range (20%-30%), yet a clear positive dependence between the mean turning rate, $\langle|\omega|\rangle$ and t_{turn} is observed, see Fig. 6. In short, the cells that turn faster also tend to turn for a longer period of time.

DISCUSSION

In this work, we demonstrate a framework to assess how adherent cells turn. On an ensemble level, the cells' turning kinematics (under a given condition) feature a nearly constant turning rate but stochastic turning signs. When cells undertake targeted migration, they bias the signs towards the stimuli. Separating turns and runs with our protocol and analyzing the states respectively brings new insights. The analysis of runs provides a solid and nuanced support for the UCSP model [5]; while the analysis of turns evidences the hypothesized positive feedback between turning rate and duration [6]. Lastly, while adherent eukaryotic cells clearly exhibit runner-rotor kinematics, non-adherent cells such as immune cells migrate with run-and-tumble kinematics [7] — their turns are purely diffusion-driven. This distinction highlights the role of a eukaryotic cell's mechanical interactions with the substrate in determining its turning mechanism.

Two remarks must be made about the claim of 'turning at a constant rate'. (1) One should not confuse turning at a constant rate with circling, where 'circling' describes a track's turning fraction resembling a circular arc. This is because circling requires not only constant-rate turning but also a near-constant speed of forward motion. However, the propagation speed u_{\parallel} of our cells varies strongly over time, which constitutes the probability distributions displayed in Figs. 1(c), 4(c), and 4(h). With Fig. ?? in Appendix A, we further demonstrate this point with typical tracks with long turning events: the appearance of these turns is disparate from a circle or an arc. Nevertheless, circling behaviors do exist. They have been reported in fish keratocytes, which migrate $\sim 10\times$ faster than the cells studied here and have distinct morphologies [6]. (2) On the scale of single turns, single cells,

and the ensemble, 'turning at a constant rate' means differently. Per single turn, we observe that there exists a constant rate that does not vary over time, Fig. 2(a). Per single cell, the rates for each of its turns are stochastically determined, from approximately the same probability distribution as the ensemble, Fig. ??(a). On the ensemble level, the constant-rate turning manifests as a linear trend between the most probable angular change ($\langle\Psi\rangle$) of a turn and its duration (t_{turn}), see Figs. 2(c) 4(d), and 4(i).

Considering how much the cell's properties (e.g. morphology, speed, size) vary from one to another within a population, the existence of a most probable rate of turning is surprising and has crucial implications for modeling the kinematics of adherent cell migration. Previously, the turning dynamics are typically understood as a diffusive process [5, 12], where $\phi(t) \sim \zeta(t)$, with ζ a zero-mean Gaussian noises. However, our results indicate that turnings should be described as:

$$\dot{\phi} = \Omega + \zeta(t), \quad (2)$$

where Ω accounts for the deterministic turning. The two descriptions of turning are fundamentally different.

Lastly, to explain the kinematics described in Eq. (2), we combine the insights from Ref. [8] and Ref. [6]. In runs, only actin filaments perpendicular to the cell membrane would polymerize fast enough to stay in contact with the forward-moving membrane. The actin flow and the membrane motion reinforce each other, such that the direction of run dominates the actin flows. However, at a certain point, when the actin flow is not strong enough to push the cell forward, the direction of actin filament polymerization would bifurcate. At this instant, the likelihood of both leftwards and rightwards actin flow - and consequently, the cell's turning left or right - is symmetric. However, due to positive feedback between polymerization and membrane deformation and the limited source of actins, the left-right symmetry will break: one turning direction will out-compete the other and lead the cells to turn [8]. After the symmetry-break, accumulation of myosin-II at the outer and rear side and the asymmetric actin flow start mutually enhancing each other [6]. This positive feedback probably sustains the turning at a near constant rate. However, what sets the mean turning rate over a population of cells remains to be clarified. Future experiments are called for to elucidate this question.

MATERIALS AND METHODS

Cell culture

Non-tumorigenic epithelial cells (MCF-10A) cells are cultured in DMEM/F12 (Sigma-Aldrich and Invitrogen) at 37°C in a 5% CO₂ atmosphere. Supplements added

Cell	Number $N=$	Substrate (min)	τ_{turn} (min)	τ_{run} (min)	Ω_{turn} (rad/min)	$D_{r,\text{turn}}$ (min^{-1})	$D_{r,\text{run}}$ (min^{-1})
MCF-10A	396	collagen	8.2	29.9	0.160 (0.160)	0.031	0.005
MCF-10A	318	PDMS	18.5	60.4	0.083 (0.090)	0.006	0.004
NIH-3T3	280	PDMS	12.3	68.4	0.082 (0.086)	0.011	0.005

TABLE I. Kinematics properties for different cells. $\tau_{\text{run,turn}}$ is obtained from exponential fitting the state interval distributions; Ω_{turn} and $D_{r,\text{run,turn}}$ are obtained from fitting the ACF with Eq. (1). The values in parenthesis (\cdot) represent results of linear fitting of $\langle \Psi \rangle$ with $t_{\text{run,turn}}$.

549 to the media include 5% horse serum (Kang Yuan Biol-
 ogy and Invitrogen), Pen/Strep (100 \times solution, Gibco,⁵⁹¹
 1% v/v), EGF (20 ng/ml, Peprotech), Hydrocortisone
 552 (0.5 $\mu\text{g}/\text{ml}$, Sigma-Aldrich), Cholera toxin (100 ng/ml,
 Sigma-Aldrich), and Insulin (10 $\mu\text{g}/\text{ml}$, Sigma-Aldrich).⁵⁹⁴

555 Fibroblasts (NIH-3T3) are cultured in DMEM (Corn-
 ing) supplemented with 10% bovine calf serum (GIBCO)
 and 1% penicillin-streptomycin (100 \times solution, Invitro-
 gen) at 37 $^{\circ}\text{C}$ in a 5% CO_2 atmosphere.

558 The MCF-10A cells examined on collagen substrates⁵⁹⁷
 are kindly provided by Yang Gen Lab, Peking Univer-
 sity, China; while the MCF-10A and NIH-3T3 cells ex-
 561 amined on PDMS substrates are obtained from the Chi-
 nese National Biomedical Cell-Line Resource. The latter
 group of MCF-10A cells express a green fluorescent pro-
 564 tein (GFP) and the NIH-3T3 cells are labeled with GFP
 through transduction of HBLV-ZsGreen-PURO (Han-
 bio).⁶⁰³

567 Preparation of PDMS substrates

The silicone elastomer PDMS (Sylgard 184, Dow Corn-⁶⁰⁹
 ing) is cast on a dish and cured at 60 $^{\circ}\text{C}$ for 4 h (base
 570 stiffness ~ 750 kPa). The substrate is rinsed with ethanol
 and blown dry with nitrogen gas. The substrate surface⁶¹²
 is further oxidized by air plasma clean (Harrick Plasma)
 573 and coated with fibronectin (50 $\mu\text{g}/\text{mL}$, Sigma) in DPBS
 to enhance cell adhesion.⁶¹⁵

Motility assays

576 200 μl MCF-10A cell suspension (1×10^4 ml^{-1}) is de-
 posited onto a 2 mg/ml collagen gel substrate in a 14 mm⁶²¹
 well, incubated overnight, and observed thereafter. Im-
 579 ages are taken every 2 min for 6 hour. We focus on single
 cell migration and thus stop tracking when the cell at-
 taches to another or divides into two. We further exclude
 582 the tracks that exhibit low motility (i.e. the maximum
 displacement during the entire recording is less than 45⁶²⁴
 μm , ~ 1.5 cell size). Finally, $N=396$ (out of 518) MCF-
 585 10A tracks on collagen are collected. Tracking is based on
 template matching with customized software [OpenCV-⁶²⁷
 python package (ver.4.5.1)].

588 MCF-10A and NIH-3T3 observed on PDMS substrates
 are observed and tracked with fluorescence microscopy.⁶³⁰

Cell suspensions of 1×10^5 ml^{-1} concentration are used
 and observation starts 6 h later. Images are taken every
 4 min for 12 hours. The software Imaris is used to track
 the time-dependent positions of the centroids of individ-
 ual cells.

All cells are observed in their maintaining condition
 with an inverted microscope (Nikon, Eclipse Ti).

Mechanotaxis assays

Needles held by a motorized micromanipulator (Ep-
 pendorf, InjectMan 4) and inserted into the collagen gel
 substrate to perform cyclic stretching. The needle is
 placed 60 μm to the right of the targeted cell ($+x$ -axis).
 It enters 50 μm deep into the substrate, and pulls the
 substrate 30 μm away from the cell. A stretch cycle con-
 sists of the following phases: pull (10 $\mu\text{m}/\text{s}$), hold (30 s,
 60 s, or ∞), release (50 $\mu\text{m}/\text{s}$), and return (to the initial
 position, 100 $\mu\text{m}/\text{s}$). The collagen gel used is uniformly
 mixed with 0.013% w/v microbeads (0.87 μm diameter,
 Spherotech, FP-0856-2), which help track the gel defor-
 mation. In the mechanotaxis assays, MCF-10A cells are
 tracked manually and the gel deformation is subtracted
 from the track.

Cells are observed following the same protocol for
 motility assays. MCF-10A cell suspension of a lower den-
 sity (5×10^3 ml^{-1}) is employed. Prior to the application
 of mechanical stimuli, the cells' motility are monitored
 for 20 minutes. Approximately half of the cells are found
 to be amoebic and in the 'run' state. Among the motile
 ones, a cell moving at an angle ϕ between $\frac{\pi}{6}$ and $\frac{\pi}{2}$
 with respect to the $+x$ -axis is randomly chosen for mechano-
 taxis assay. Cells under different cyclic stretching ($N \approx 30$
 for each group) are qualitatively the same and are there-
 fore combined. $N=93$ cells are eventually recruited.

Methods

The ACFs of turns presented in Figs. 2(e), 4(d), and
 4(j) are obtained by averaging over multiple single-turn
 ACFs. As the turns last for different lengths of time,
 each scatter point on the graph may represent an average
 value derived from samples of varying sizes. The data
 is truncated at the time interval Δt if the number of
 available turns are less than $N = 10$ [Figs. 2(e)] or less

than $N = 5$ [Figs. 4(d) and 4(j)].

The aspect ratio, AR, of a given cell is reported as follows. First, with image analysis we obtain the cell's contour for each frame of video. For each frame, we compute the aspect ratio of the smallest bounding box of the cell's contour, $AR(t)$. Lastly, AR is reported as the mean of $AR(t)$ over the entire track duration.

In mechanotaxis assays, the temporal distribution of turns of arrived cells in Fig. 3(e) is adjusted to account for the varying sample size (number of tracks) over time. The number of available tracks decreases over time as more and more cells have arrived at the pipette and their tracks have ended. To account for this, we present the adjusted temporal distribution of turns $PDF^* = PDF/\gamma(t)$, where the coefficient $\gamma(t) \equiv N(t)/N(0)$ and $N(t)$ denotes the number of still available tracks at time t . Moreover, the data is truncated at $t \approx 100$ min as there are less than $N = 10$ remaining tracks afterwards.

In studying the correlation between event duration and the mean (angular) speed (Figs. 5 and 6), data are binned by event duration (t_{run} or t_{turn}) and the latter is presented as the x -axis. We avoid binning by the mean speed during an event. This is because extremely large (angular) speeds induced by transient fluctuations (e.g., mor-

phological changes), are more likely to dominate short events. Therefore, instead of averaging out the effect of noise, binning by speed actually highlights the noise, especially at large speeds.

ACKNOWLEDGEMENTS

We thank Hui Li and Mingcheng Yang for helpful discussions. This work is supported by the National Key Research and Development Program of China (2022YFA1405002); the National Natural Science Foundation of China (NSFC) (Grant Nos. 12204525, 12325405, 12090054); the Youth Innovation Promotion Association of CAS (No. 2021007).

AUTHOR CONTRIBUTIONS

Y.Z. and X.Y. performed experiments; Q.F. and F.Y. designed experiments; B.Z. and D.W. performed simulations; D.W. analyzed data and wrote the manuscript. D.W. and F.Y. conceived and supervised the project. All authors reviewed the manuscript.

-
- [1] Trepant, X., Chen, Z. & Jacobson, K. *Cell Migration*, 2369–2392 (John Wiley & Sons, Ltd, 2012).
- [2] Gail, M. H. & Boone, C. W. The locomotion of mouse fibroblasts in tissue culture. *Biophys. J.* **10**, 980–993 (1970).
- [3] Hall, R. L. Amoeboid movement as a correlated walk. *J. Math. Biol.* **4**, 327–335 (1977).
- [4] Murrell, M., Oakes, P. W., Lenz, M. & Gardel, M. L. Forcing cells into shape: the mechanics of actomyosin contractility. *Nat. Rev. Mol. Cell Biol.* **16**, 486–498 (2015).
- [5] Maiuri, P. *et al.* Actin flows mediate a universal coupling between cell speed and cell persistence. *Cell* **161**, 374–386 (2015).
- [6] Allen, G. M. *et al.* Cell mechanics at the rear act to steer the direction of cell migration. *Cell Syst.* **11**, 286–299.e4 (2020).
- [7] Zhang, Y. *et al.* Run-and-tumble dynamics and mechanotaxis discovered in microglial migration. *Research* **6**, 0063 (2023).
- [8] Jiang, C. *et al.* Switch of cell migration modes orchestrated by changes of three-dimensional lamellipodium structure and intracellular diffusion. *Nat. Commun.* **14**, 5166 (2023).
- [9] Berg, H. C. & Brown, D. A. Chemotaxis in *Escherichia coli* analysed by three-dimensional tracking. *Nature* **239**, 500–504 (1972).
- [10] Abaurra Velasco, C., Dehghani Ghahnaviyeh, S., Nejat Pishkenari, H., Auth, T. & Gompper, G. Complex self-propelled rings: a minimal model for cell motility. *Soft Matter* **13**, 5865–5876 (2017).
- [11] Xie, L., Altindal, T., Chattopadhyay, S. & Wu, X.-L. Bacterial flagellum as a propeller and as a rudder for efficient chemotaxis. *Proc. Natl. Acad. Sci. U.S.A.* **108**, 2246–2251 (2011).
- [12] Alessandro, J. *et al.* Contact enhancement of locomotion in spreading cell colonies. *Nat. Phys.* **13**, 999–1005 (2017).
- [13] Shaebani, M. R., Jose, R., Santen, L., Stankevics, L. & Lautenschläger, F. Persistence-speed coupling enhances the search efficiency of migrating immune cells. *Phys. Rev. Lett.* **125**, 268102 (2020).
- [14] Werner, M., Petersen, A., Kurniawan, N. A. & Bouten, C. V. C. Cell-perceived substrate curvature dynamically coordinates the direction, speed, and persistence of stromal cell migration. *Adv. Biosyst.* **3**, 1900080 (2019).
- [15] Begemann, I. *et al.* Mechanochemical self-organization determines search pattern in migratory cells. *Nat. Phys.* **15**, 848–857 (2019).
- [16] Potdar, A. A., Lu, J., Jeon, J., Weaver, A. M. & Cummings, P. T. Bimodal analysis of mammary epithelial cell migration in two dimensions. *Ann. Biomed. Eng.* **37**, 230–245 (2009).
- [17] Alon, U. *et al.* Response regulator output in bacterial chemotaxis. *EMBO J.* **17**, 4238–4248 (1998).
- [18] Runs longer than ~ 150 min seem to follow either another exponential distribution with larger characteristic time (~ 80 min) or a long tail (e.g., power-law) distribution.
- [19] Lämmermann, T. & Sixt, M. Mechanical modes of 'amoeboid' cell migration. *Curr. Opin. Cell Biol.* **21**, 636–644 (2009).
- [20] Friedl, P. & Wolf, K. Plasticity of cell migration: a multiscale tuning model. *J. Cell Biol.* **188**, 11–19 (2010).
- [21] Pollard, T. D. & Borisy, G. G. Cellular motility driven by assembly and disassembly of actin filaments. *Cell* **112**, 453–465 (2003).

- [22] Jerison, E. R. & Quake, S. R. Heterogeneous t cell motility behaviors emerge from a coupling between speed and turning in vivo. *Elife* **9**, e53933 (2020).⁷⁴⁷
- [23] Leineweber, W. D. & Fraley, S. I. Adhesion tunes speed and persistence by coordinating protrusions and extracellular matrix remodeling. *Dev. Cell* **58**, 1414–1428.e4750⁷⁴⁴
- [24] (2023). The curve of $T_{\text{turn}}/T_{\text{tot}}$ can also be fitted well by a mixture of two exponential distributions, whose characteristic scales help determine Ω_c . However, fitting with the mixed exponential functions is more sensitive to small variation in data. It is thus deemed less robust and not employed.